

A simple thermopiezoelastic model for smart composite plates with accurate stress recovery*

Wenbin Yu¹ and Dewey H Hodges^{2,3}

¹ Department of Mechanical and Aerospace Engineering, Utah State University, Logan, UT 84341-4130, USA

² School of Aerospace Engineering, Georgia Institute of Technology, Atlanta, GA 30332-0150, USA

E-mail: dewey.hodges@ae.gatech.edu

Received 6 June 2003, in final form 29 March 2004

Published 23 June 2004

Online at stacks.iop.org/SMS/13/926

doi:10.1088/0964-1726/13/4/031

Abstract

A Reissner–Mindlin model for analyzing laminated composite plates including piezoelectric layers under mechanical, thermal and electric loads has been constructed using the variational-asymptotic method. The present work formulates the original nonlinear, three-dimensional, one-way coupled, thermopiezoelasticity problem allowing for arbitrary deformation of the normal line and using a set of intrinsic variables defined on the reference plane. The variational-asymptotic method is used to rigorously split the three-dimensional problem into two problems: a nonlinear, two-dimensional, plate analysis over the reference plane to obtain the global deformation, and a linear analysis through the thickness to provide both the two-dimensional generalized constitutive model and recovery relations to approximate the original three-dimensional results. The obtained asymptotically correct second-order electric enthalpy is cast into the form of the commonly used Reissner–Mindlin model to account for transverse shear deformation. The present theory is implemented into the computer program VAPAS (variational-asymptotic plate and shell analysis). Results for several cases obtained from VAPAS are compared with the exact thermopiezoelasticity solutions, classical lamination theory and first-order shear–deformation theory for the purpose of demonstrating the advantages of the present theory and the use of VAPAS. The proposed theory can achieve an accuracy comparable to higher-order layerwise theories at the cost of a first-order shear–deformation theory.

1. Introduction

Research in smart structures has received enormous attention in recent years [1–5]. Smart structures are capable of sensing and reacting to external disturbances and thus create the

possibility of building structures that are self-monitorable and self-controllable. Such smart structures are promising candidates to meet the demanding requirements of high-strength, high-stiffness and light-weight structures for modern engineering, especially aerospace applications. Among many possible candidates for actuators and sensors, piezoelectrics receive the most attention. One reason for this preference is that piezoelectrics can directly relate electric signals to strain components in the material and vice versa. Thus, they can

* Presented at the 44th Structures, Structural Dynamics and Materials Conference, Norfolk, VA, 7–10 April 2003.

³ Formerly at: School of Aerospace Engineering, Georgia Institute of Technology, Atlanta, GA 30332-0150, USA.

be used both as actuators and sensors. Moreover, in most cases, piezoelectrics are used along with tailored anisotropic materials to maximize the intelligence of a smart structure. While most research has been focused on the behavior of piezoelectric structures under isothermal conditions, an increasing effort has been directed to address thermal-piezoelectric-mechanical response [6–8].

Many smart structures have one dimension much smaller than the other two and can be modeled as plates if there are no initial curvatures associated with the plane formed by the two large dimensions. The current capability of analyzing thermopiezoelectric behavior of smart plates is limited. The mathematical models are generally derived from three-dimensional (3D) thermopiezoelectricity theory, making use of the fact that the thickness is small in some sense. Most analyses prevailing in the literature are ad hoc theories, which can be generally classified as classical lamination theories (CLT) [9], first-order shear-deformation theories (FOSDT) [10], higher-order theories [8], zig-zag theories [11] and layerwise theories [12]. Layerwise theories can produce reasonable results at the cost of complex models and expensive computation. Zig-zag theories yield good results for some problems, but since they have not been proved to be asymptotically correct they may fail for some cases. All the other ad hoc approaches are doomed to fail, especially for stress prediction through the thickness of layered plates, even for thin ones. The reason is that these theories assume the displacement variables to be C^∞ functions, while in reality the displacement field of a layered plate may have discontinuous derivatives through the thickness.

Physically we limit our theory to the case of small strain. From a mathematical point of view, the remaining approximations in the analysis stem from elimination of the thickness coordinate from the independent variables of the governing equations of motion for the plate structure. This sort of approximation is inevitable if one wants to take advantage of the small thickness to simplify the analysis. However, other approximations that are not absolutely necessary should be avoided. For example, for small-strain analysis of plates, it is reasonable to assume that the thickness, h , is small compared to the wavelength of deformation of the reference plane, l . However, it is not at all reasonable to assume *a priori* some ad hoc displacement field, although that is the way most existing plate theories have been constructed.

A simple and accurate model of composite plates and shells based on the variational-asymptotic method (VAM) [17] has been under development over the last few years [13–16] along with a corresponding computer program, the variational-asymptotic plate and shell analysis (VAPAS). VAPAS starts with the formulation of the 3D anisotropic elasticity problem in which the deformation of the reference surface is expressed in terms of intrinsic two-dimensional (2D) variables. The intrinsic formulation allows the body to undergo arbitrarily large displacement and global rotation subject only to the restriction that the generalized 2D strains are small. VAM is then used to systematically reduce the dimensionality of the problem by taking advantage of the small parameters inherent in the problem. The original nonlinear 3D problem is thus mathematically split into a linear one-dimensional (1D) through-the-thickness analysis and a nonlinear 2D plate/shell

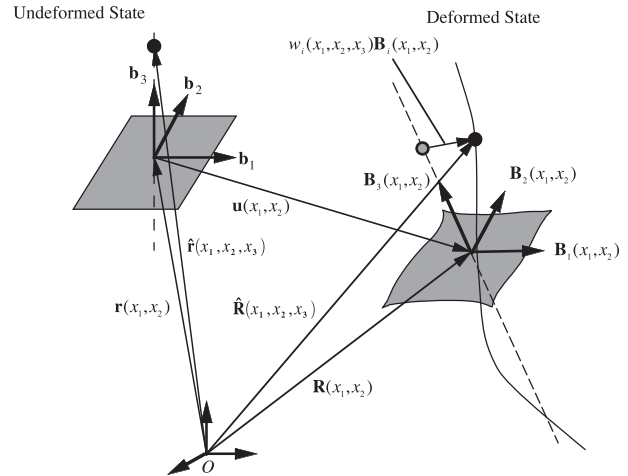


Figure 1. Schematic of the plate deformation.

analysis accounting for transverse shear deformation. The through-the-thickness analysis is solved by the finite element method and provides a constitutive model between the generalized, 2D strains and stress resultants as well as recovery relations to accurately approximate the 3D displacement, strain and stress fields in terms of 2D variables calculated in the 2D plate/shell analysis. Numerical examples presented in previous publications related with VAPAS [13–16] have demonstrated for mechanical and thermal loading that although the resulting theory is as simple as a single-layer FOSDT, the recovered 3D displacement, strain and stress results have an accuracy comparable to that of higher-order, layer-wise theories with many more degrees of freedom.

The present work extends VAPAS so that the thermopiezoelectric effects of smart plates can be treated in the same framework. Because the procedure is quite similar, the authors have chosen to repeat some formulae and text from their previous publications in order to make the present paper more self-contained. The present theory has been implemented into the computer program VAPAS, and now one can use this program along with a 2D plate solver to carry out an accurate and efficient thermopiezoelectric analysis for smart composite plates actuated by piezoelectrics.

2. 3D formulation

A point in the plate can be described by its Cartesian coordinates x_i (see figure 1), where x_α are two orthogonal lines in the reference plane and x_3 is the normal coordinate. (Here and throughout the paper, Greek indices assume values 1 and 2 while Latin indices assume 1, 2 and 3. Repeated indices are summed over their range except where explicitly indicated.) Letting \mathbf{b}_i denote the unit vector along x_i for the undeformed plate, one can then describe the position of any material point in the undeformed configuration by its position vector $\hat{\mathbf{r}}$ from a fixed point O , such that

$$\hat{\mathbf{r}}(x_1, x_2, x_3) = \mathbf{r}(x_1, x_2) + x_3 \mathbf{b}_3 \quad (1)$$

where \mathbf{r} is the position vector from O to the point located by x_α on the reference plane. When the origin of the coordinate

system is located on the middle plane, we have

$$\langle \hat{\mathbf{r}}(x_1, x_2, x_3) \rangle = \mathbf{r}(x_1, x_2) \quad (2)$$

where the angle brackets denote the definite integral through the thickness of the plate and will be used throughout the rest of the development.

When the plate deforms, the particle that had position vector $\hat{\mathbf{r}}$ in the undeformed configuration now has position vector $\hat{\mathbf{R}}$ in the deformed configuration. The latter can be uniquely determined by the deformation of the 3D body. Analogous to \mathbf{b}_i for the undeformed state, another triad \mathbf{B}_i is introduced for the deformed configuration. The relation between \mathbf{B}_i and \mathbf{b}_i can be specified by an arbitrarily large rotation specified in terms of the matrix of direction cosines $C(x_1, x_2)$ so that

$$\mathbf{B}_i = C_{ij} \mathbf{b}_j \quad C_{ij} = \mathbf{B}_i \cdot \mathbf{b}_j \quad (3)$$

subject to the requirement that \mathbf{B}_i is coincident with \mathbf{b}_i when the plate surface is undeformed. Now the position vector $\hat{\mathbf{R}}$ can be represented as

$$\hat{\mathbf{R}}(x_1, x_2, x_3) = \mathbf{R}(x_1, x_2) + x_3 \mathbf{B}_3(x_1, x_2) + w_i(x_1, x_2, x_3) \mathbf{B}_i(x_1, x_2) \quad (4)$$

where w_i is the warping of the normal-line element. In the present work, the form of the warping w_i is not assumed, as in most plate theories. Rather, these quantities are treated as unknown 3D functions and will be solved for later.

Because of the way warping is introduced, equation (4) is six times redundant, so that six constraints are needed to make the formulation unique. The redundancy can be removed by choosing appropriate definitions of \mathbf{R} and \mathbf{B}_i . One can define \mathbf{R} similarly as equation (2) to be the average position through the thickness, from which it follows that the warping functions must satisfy the following three constraints:

$$\langle w_i(x_1, x_2, x_3) \rangle = 0. \quad (5)$$

Two additional constraints can be specified by taking \mathbf{B}_3 as the normal to the deformed reference plane. It should be noted that this choice has nothing to do with the Kirchhoff hypothesis. In the Kirchhoff assumption, no local deformation of the transverse normal is allowed. However, according to the present scheme we allow all possible deformations, classifying all deformations other than that of CLT as warping, which is assumed to be small. This assumption is valid if the strain is small and if the local rotation (i.e. the rotation of a normal line element caused by warping) is not larger than the order of the strain [18].

Based on the concept of decomposition of the rotation tensor [19], the Jauman–Biot–Cauchy strain components for small local rotation are given by

$$\Gamma_{ij} = \frac{1}{2}(F_{ij} + F_{ji}) - \delta_{ij} \quad (6)$$

where F_{ij} is the mixed-basis component of the deformation gradient tensor such that

$$F_{ij} = \mathbf{B}_i \cdot \mathbf{G}_k \mathbf{g}^k \cdot \mathbf{b}_j. \quad (7)$$

Here

$$\mathbf{G}_k = \frac{\partial \hat{\mathbf{R}}}{\partial x_k}$$

are the covariant basis vectors of the deformed configuration and \mathbf{g}^k the contravariant base vectors of the undeformed configuration and $\mathbf{g}^k = \mathbf{g}_k = \mathbf{b}_k$. One can obtain \mathbf{G}_k with the help of the definition of so-called generalized 2D strains similarly as [20], given by

$$\mathbf{R}_{,\alpha} = \mathbf{B}_\alpha + \varepsilon_{\alpha\beta} \mathbf{B}_\beta \quad (8)$$

$$\mathbf{B}_{i,\alpha} = (-K_{\alpha\beta} \mathbf{B}_\beta \times \mathbf{B}_3 + K_{\alpha 3} \mathbf{B}_3) \times \mathbf{B}_i \quad (9)$$

where $\varepsilon_{\alpha\beta}$ and $K_{\alpha\beta}$ are the 2D generalized strains and comma denotes the differentiation with respect to the coordinates. Here one is free to set $\varepsilon_{12} = \varepsilon_{21}$, i.e.

$$\mathbf{B}_1 \cdot \mathbf{R}_{,2} = \mathbf{B}_2 \cdot \mathbf{R}_{,1} \quad (10)$$

which can serve as another constraint to specify the deformed configuration.

With the assumption that the strain is small compared to unity, which has the effect of removing all the terms that are products of the warping and the generalized strains, one can express the 3D strain field as

$$\Gamma = \Gamma_h w + \Gamma_\epsilon \epsilon + \Gamma_{l_1} w_{,1} + \Gamma_{l_2} w_{,2} \quad (11)$$

where

$$\Gamma = [\Gamma_{11} \quad 2\Gamma_{12} \quad \Gamma_{22} \quad 2\Gamma_{13} \quad 2\Gamma_{23} \quad \Gamma_{33}]^T \quad (12)$$

$$w = [w_1 \quad w_2 \quad w_3]^T \quad (13)$$

$$\epsilon = [\varepsilon_{11} \quad 2\varepsilon_{12} \quad \varepsilon_{22} \quad K_{11} \quad K_{12} + K_{21} \quad K_{22}]^T \quad (14)$$

and all the operators are defined as:

$$\Gamma_h = \begin{bmatrix} 0 & 0 & 0 \\ 0 & 0 & 0 \\ 0 & 0 & 0 \\ \frac{\partial}{\partial x_3} & 0 & 0 \\ 0 & \frac{\partial}{\partial x_3} & 0 \\ 0 & 0 & \frac{\partial}{\partial x_3} \end{bmatrix} \quad \Gamma_{l_1} = \begin{bmatrix} 1 & 0 & 0 \\ 0 & 1 & 0 \\ 0 & 0 & 0 \\ 0 & 0 & 1 \\ 0 & 0 & 0 \\ 0 & 0 & 0 \end{bmatrix} \quad (15)$$

$$\Gamma_\epsilon = \begin{bmatrix} 1 & 0 & 0 & x_3 & 0 & 0 \\ 0 & 1 & 0 & 0 & x_3 & 0 \\ 0 & 0 & 1 & 0 & 0 & x_3 \\ 0 & 0 & 0 & 0 & 0 & 0 \\ 0 & 0 & 0 & 0 & 0 & 0 \\ 0 & 0 & 0 & 0 & 0 & 0 \end{bmatrix} \quad \Gamma_{l_2} = \begin{bmatrix} 0 & 0 & 0 \\ 1 & 0 & 0 \\ 0 & 1 & 0 \\ 0 & 0 & 0 \\ 0 & 0 & 1 \\ 0 & 0 & 0 \end{bmatrix}. \quad (16)$$

In the present work, we only study the actuated effect caused by applied thermal or electric loads, which means there is only one-way thermopiezoelastic coupling. The changes of temperature and electric fields caused by deformation of the plate are negligible, and any interactions between temperature and electric fields are not considered. Thus, we can use the electric enthalpy without the quadratic terms involving temperature and/or electric fields to carry out the analysis. The enthalpy per unit area (which is the same as the enthalpy of a normal line element) can be written as

$$U = (\frac{1}{2} \Gamma^T D \Gamma - \Gamma^T D \alpha T - \Gamma^T D d \mathcal{E}) \quad (17)$$

where T is the difference of temperature inside the structure with respect to the reference temperature when the plate is

stress free, \mathcal{E} is the electric field vector, D is the 3D 6×6 material matrix, which consists of elements of the elasticity tensor expressed in the global coordinate system x_i , α is a 6×1 column matrix representing the 3D thermal expansion coefficients and d is a 6×3 matrix representing the 3D strain–piezoelectric coefficients. These matrices are in general fully populated. However, if it is desired to model laminated composite plates in which each lamina exhibits a monoclinic symmetry about its own mid-plane and is rotated about the local normal to be a layer in the laminated composite plate, some parts of D will always vanish [13] no matter what the layup angle is, and α and d will assume the following forms:

$$\alpha = [\alpha_{11} \quad 2\alpha_{12} \quad \alpha_{22} \quad 0 \quad 0 \quad \alpha_{33}]^T \quad (18)$$

$$d = \begin{bmatrix} 0 & 0 & d_{113} \\ 0 & 0 & 2d_{123} \\ 0 & 0 & d_{223} \\ 2d_{131} & 2d_{132} & 0 \\ 2d_{231} & 2d_{232} & 0 \\ 0 & 0 & d_{333} \end{bmatrix}. \quad (19)$$

To deal with applied mechanical loads, we will at first leave open the existence of a potential and develop instead the virtual work of applied mechanical loads. The virtual displacement is taken as the Lagrangean variation of the displacement field, such that

$$\delta \hat{\mathbf{R}} = \overline{\delta q}_{Bi} \mathbf{B}_i + x_3 \delta \mathbf{B}_3 + \delta w_i \mathbf{B}_i + w_i \delta \mathbf{B}_i \quad (20)$$

where the virtual displacement of the reference plane is given by

$$\overline{\delta q}_{Bi} = \delta \mathbf{u} \cdot \mathbf{B}_i \quad (21)$$

and the virtual rotation of the reference plane is defined such that

$$\delta \mathbf{B}_i = (-\overline{\delta \psi}_{B\beta} \mathbf{B}_\beta \times \mathbf{B}_3 + \overline{\delta \psi}_{B3} \mathbf{B}_3) \times \mathbf{B}_i. \quad (22)$$

Since the strain is small, one may safely ignore products of the warping and the loading in the virtual rotation term. Then, the work done through a virtual displacement by the applied loads $\tau_i \mathbf{B}_i$ at the top surface, $\beta_i \mathbf{B}_i$ at the bottom surface, and the body force $\phi_i \mathbf{B}_i$ through the thickness is

$$\overline{\delta W} = (\tau_i + \beta_i + \langle \phi_i \rangle) \overline{\delta q}_{Bi} + \overline{\delta \psi}_{B\alpha} \left[\frac{h}{2} (\tau_\alpha - \beta_\alpha) + \langle x_3 \phi_\alpha \rangle \right] + \delta (\tau_i w_i^+ + \beta_i w_i^- + \langle \phi_i w_i \rangle) \quad (23)$$

where τ_i , β_i and ϕ_i are taken to be independent of the deformation, $(\)^+ = (\)|_{x_3=\frac{h}{2}}$, and $(\)^- = (\)|_{x_3=-\frac{h}{2}}$. By introducing column matrices $\overline{\delta q}$, $\overline{\delta \psi}$, τ , β and ϕ , which are formed by stacking the three elements associated with indexed symbols of the same names, one may write the virtual work in matrix form, so that

$$\overline{\delta W} = \overline{\delta q}^T f + \overline{\delta \psi}^T m + \delta (\tau^T w^+ + \beta^T w^- + \langle \phi^T w \rangle) \quad (24)$$

where

$$f = \tau + \beta + \langle \phi \rangle$$

$$m = \begin{Bmatrix} \frac{h}{2} (\tau_1 - \beta_1) + \langle x_3 \phi_1 \rangle \\ \frac{h}{2} (\tau_2 - \beta_2) + \langle x_3 \phi_2 \rangle \\ 0 \end{Bmatrix}. \quad (25)$$

The complete statement of the problem can now be presented in terms of the principle of virtual work, such that

$$\delta U - \overline{\delta W} = 0. \quad (26)$$

In spite of the possibility of accounting for nonconservative forces in the above, the problem that governs the warping is conservative when τ_i , β_i and ϕ_i are taken to be independent of the deformation. Thus, one can pose the problem that governs the warping as the minimization of a total potential functional

$$\Pi = U - W \quad (27)$$

so that

$$\delta \Pi = 0 \quad (28)$$

in which only the warping displacement is varied, subject to the constraints equation (5). This implies that the work done of the applied mechanical loads for the functional governing warping is given by

$$W = \tau^T w^+ + \beta^T w^- + \langle \phi^T w \rangle. \quad (29)$$

It is obvious from energy principles that the unknown warping functions correspond to the stationary points of the functional in equation (27) subject to the constraints of equation (5). Up to this point, the derivation is simply an alternative formulation of the original 3D thermopiezoelectricity problem. If we attempt to solve this problem directly, we will meet the same difficulty as solving any full 3D problem. Fortunately, the VAM can be used to calculate the 3D warping functions asymptotically. Although the through-the-thickness analysis is 1D and can be solved analytically [13], we prefer to use the finite element method to solve the minimization problem for the sake of dealing with multiple layers and arbitrary monoclinic materials, and connecting with standard 2D plate solvers, which are normally implemented using the finite element method. Discretizing the transverse normal line into 1D finite elements, one can express the warping field as

$$w(x_i) = S(x_3) V(x_1, x_2) \quad (30)$$

where S is the shape function and V is the nodal value of warping field along the transverse normal. Substituting equation (30) into equation (27), one can express the electric enthalpy in discretized form as

$$2\Pi = V^T E V + 2V^T (D_{h\epsilon\epsilon} + D_{hl_1} V_{,1} + D_{hl_2} V_{,2}) + \epsilon^T D_{\epsilon\epsilon} \epsilon + V_{,1}^T D_{l_1 l_1} V_{,1} + V_{,2}^T D_{l_2 l_2} V_{,2} + 2(V_{,1}^T D_{l_1 \epsilon} \epsilon + V_{,2}^T D_{l_2 \epsilon} \epsilon + V_{,1}^T D_{l_1 l_2} V_{,2}) - 2V^T \alpha_h - 2\epsilon^T \alpha_\epsilon - 2V_{,1}^T \alpha_{l_1} - 2V_{,2}^T \alpha_{l_2} - 2V^T \mathcal{E}_h - 2\epsilon^T \mathcal{E}_\epsilon - 2V_{,1}^T \mathcal{E}_{l_1} - 2V_{,2}^T \mathcal{E}_{l_2} + 2V^T L \quad (31)$$

where L contains the load-related terms such that

$$L = -S^{+T} \tau - S^{-T} \beta - \langle S^T \phi \rangle. \quad (32)$$

The new matrix variables carry the properties of both the geometry and material:

$$\begin{aligned}
 E &= \langle [\Gamma_h S]^T D [\Gamma_h S] \rangle & D_{h\epsilon} &= \langle [\Gamma_h S]^T D \Gamma_\epsilon \rangle \\
 D_{hl_1} &= \langle [\Gamma_h S]^T D [\Gamma_{l_1} S] \rangle & D_{hl_2} &= \langle [\Gamma_h S]^T D [\Gamma_{l_2} S] \rangle \\
 D_{\epsilon\epsilon} &= \langle \Gamma_\epsilon^T D \Gamma_\epsilon \rangle & D_{l_1 l_1} &= \langle [\Gamma_{l_1} S]^T D [\Gamma_{l_1} S] \rangle \\
 D_{l_1 l_2} &= \langle [\Gamma_{l_1} S]^T D [\Gamma_{l_2} S] \rangle & D_{l_2 l_2} &= \langle [\Gamma_{l_2} S]^T D [\Gamma_{l_2} S] \rangle \\
 D_{l_1 \epsilon} &= \langle [\Gamma_{l_1} S]^T D \Gamma_\epsilon \rangle & D_{l_2 \epsilon} &= \langle [\Gamma_{l_2} S]^T D \Gamma_\epsilon \rangle \\
 \alpha_h &= \langle [\Gamma_h S]^T D \alpha T \rangle & \alpha_\epsilon &= \langle \Gamma_\epsilon^T D \alpha T \rangle \\
 \alpha_{l_1} &= \langle [\Gamma_{l_1} S]^T D \alpha T \rangle & \alpha_{l_2} &= \langle [\Gamma_{l_2} S]^T D \alpha T \rangle \\
 \mathcal{E}_h &= \langle [\Gamma_h S]^T D d \mathcal{E} \rangle & \mathcal{E}_\epsilon &= \langle \Gamma_\epsilon^T D d \mathcal{E} \rangle \\
 \mathcal{E}_{l_1} &= \langle [\Gamma_{l_1} S]^T D d \mathcal{E} \rangle & \mathcal{E}_{l_2} &= \langle [\Gamma_{l_2} S]^T D d \mathcal{E} \rangle.
 \end{aligned} \tag{33}$$

The constraints of the warping functions, equation (5), can be expressed in discretized form as

$$V^T H \psi = 0 \tag{34}$$

where $H = \langle S^T S \rangle$ and ψ is the normalized kernel matrix of E such that $\psi^T H \psi = I$. Now our problem is transformed to minimize equation (31) numerically, subject to the constraints in equation (34).

3. Dimensional reduction

To rigorously reduce the original 3D problem to a 2D plate problem, one must attempt to reproduce the electric enthalpy stored in the 3D structure in a 2D formulation. This dimensional reduction can only be done approximately, and one way to do it is by taking advantage of the smallness of h/l . The small parameter ϵ , representing the order of the generalized 2D strains, has already been taken advantage of when we derive equation (11). To reduce the number of small parameters in the asymptotic analysis, it is reasonable to assume that the strains caused by temperature and electricity are of the order of ϵ . Thus, the quantities of interest assume the following orders:

$$\begin{aligned}
 \epsilon_{\alpha\beta} &\sim h k_{\alpha\beta} \sim \epsilon & f_3 &\sim \mu (h/l)^2 \epsilon & f_\alpha &\sim \mu (h/l) \epsilon \\
 m_\alpha &\sim \mu h (h/l) \epsilon & \alpha T &\sim \epsilon & d\mathcal{E} &\sim \epsilon
 \end{aligned} \tag{35}$$

where μ is the order of the elastic constants (all of which are assumed to be of the same order).

Having assessed the orders of all the interested quantities, the VAM can be used to mathematically perform a dimensional reduction of the 3D problem to a series of 2D models. This method requires one to find the leading terms of the functional according to the different orders. Since only the warping is varied, the leading terms needed are all of those terms associated with warping. For the zeroth-order approximation, these leading terms of equation (31) are

$$2\Pi_0^* = V^T E V + 2V^T D_{h\epsilon} \epsilon - 2V^T \alpha_h - 2V^T \mathcal{E}_h. \tag{36}$$

The zeroth-order warping functions, which minimize the above functional subject to constraints of equation (34), can be obtained by the usual procedure of calculus of variation as:

$$V = \hat{V}_0 \epsilon + V_T + V_\mathcal{E} = V_0. \tag{37}$$

Substituting equation (37) back into equation (31), one can obtain the electric enthalpy asymptotically correct up to the order of $\mu \epsilon^2$ as

$$2\Pi_0 = \epsilon^T A \epsilon - 2\epsilon^T N_T - 2\epsilon^T N_\mathcal{E} \tag{38}$$

with

$$\begin{aligned}
 A &= (\hat{V}_0^T D_{h\epsilon} + D_{\epsilon\epsilon}) \\
 N_T &= \alpha_\epsilon + \frac{1}{2} (\hat{V}_0^T \alpha_h - D_{h\epsilon}^T V_T) \\
 N_\mathcal{E} &= \mathcal{E}_\epsilon + \frac{1}{2} (\hat{V}_0^T \mathcal{E}_h - D_{h\epsilon}^T V_\mathcal{E}).
 \end{aligned} \tag{39}$$

Although the electric enthalpy of this approximation coincides with classical plate theories for thermopiezoelectric analysis, we have not used any ad hoc kinematic assumptions such as the Kirchhoff assumption to obtain this result. Moreover, the transverse normal strain from our zeroth-order approximation is not zero.

It is understood that our zeroth-order approximation will give the same stress results as would be obtained from CLT, so that the very important transverse stress components for analyzing the failure of smart composite plates are not available. One must carry out the next approximation so that those quantities will be available. To obtain the first-order approximation, we simply perturb the zeroth-order warping functions, such that

$$V = V_0 + V_1. \tag{40}$$

Substituting equation (40) back into equation (11) and then into equation (31), one can obtain the leading terms for the first-order approximation as

$$\begin{aligned}
 2\Pi_1^* &= V_1^T E V_1 + 2V_1^T D_1 \epsilon_{,1} + 2V_1^T D_2 \epsilon_{,2} + 2V_1^T L_T \\
 &\quad + 2V_1^T L_\mathcal{E} + 2V_1^T L
 \end{aligned} \tag{41}$$

with

$$\begin{aligned}
 L_T &= (D_{hl_1} - D_{hl_1}^T) V_{T,1} + (D_{hl_2} - D_{hl_2}^T) V_{T,2} + \alpha_{l_1,1} + \alpha_{l_2,2} \\
 L_\mathcal{E} &= (D_{hl_1} - D_{hl_1}^T) V_{\mathcal{E},1} + (D_{hl_2} - D_{hl_2}^T) V_{\mathcal{E},2} + \mathcal{E}_{l_1,1} + \mathcal{E}_{l_2,2} \\
 D_1 &= (D_{hl_1} - D_{hl_1}^T) \hat{V}_0 - D_{l_1 \epsilon} \\
 D_2 &= (D_{hl_2} - D_{hl_2}^T) \hat{V}_0 - D_{l_2 \epsilon}.
 \end{aligned} \tag{42}$$

Integration by parts with respect to the in-plane coordinates is used here and hereafter whenever it is convenient for the derivation, because the present goal is to obtain an interior solution for the plate without consideration of edge effects. Note that the treatment of edge effects is itself a very important problem to tackle, but it is outside the scope of the present work.

Similarly as in the zeroth-order approximation, one can solve the first-order warping field as

$$V_1 = V_{11} \epsilon_{,1} + V_{12} \epsilon_{,2} + V_{1T} + V_{1\mathcal{E}} + V_{1L} \tag{43}$$

and obtain an electric enthalpy that is asymptotically correct through the order of $\mu (h/l)^2 \epsilon$, given by

$$\begin{aligned}
 2\Pi_1 &= \epsilon^T A \epsilon + \epsilon_{,1}^T B \epsilon_{,1} + 2\epsilon_{,1}^T C \epsilon_{,2} + \epsilon_{,2}^T D \epsilon_{,2} - 2\epsilon^T F \\
 &\quad - 2\epsilon^T F_T - 2\epsilon^T F_\mathcal{E}
 \end{aligned} \tag{44}$$

where

$$\begin{aligned} B &= \hat{V}_0^T D_{l_1 l_1} \hat{V}_0 + V_{11}^T D_1 \\ C &= \hat{V}_0^T D_{l_1 l_2} \hat{V}_0 + \frac{1}{2}(V_{11}^T D_2 + D_1^T V_{12}) \\ D &= \hat{V}_0^T D_{l_2 l_2} \hat{V}_0 + V_{12}^T D_2 \\ F &= \frac{1}{2}(D_1^T V_{1L,1} + V_{11}^T L_{,1} + D_2^T V_{1L,2} + V_{12}^T L_{,2}) - \hat{V}_0^T L \end{aligned} \quad (45)$$

with the non-mechanical load due to temperature

$$\begin{aligned} F_T &= N_T + \hat{V}_0^T D_{l_1 l_1} V_{T,11} + \hat{V}_0^T D_{l_2 l_2} V_{T,22} \\ &+ \hat{V}_0^T (D_{l_1 l_2} + D_{l_2 l_1}^T) V_{T,12} \\ &+ \frac{1}{2}(V_{11}^T L_{T,1} + V_{12}^T L_{T,2} + D_1^T V_{1T,1} + D_2^T V_{1T,2}) \end{aligned} \quad (46)$$

and the non-mechanical load due to electric field

$$\begin{aligned} F_\varepsilon &= N_\varepsilon - \hat{V}_0^T D_{hl_1} V_{\varepsilon,1} - \hat{V}_0^T D_{hl_2} V_{\varepsilon,2} - D_{l_1 \varepsilon}^T V_{\varepsilon,1} - D_{l_2 \varepsilon}^T V_{\varepsilon,2} \\ &+ \hat{V}_0^T D_{l_1 l_1} V_{\varepsilon,11} + \hat{V}_0^T D_{l_2 l_2} V_{\varepsilon,22} + \hat{V}_0^T (D_{l_1 l_2} + D_{l_2 l_1}^T) V_{\varepsilon,12} \\ &+ \frac{1}{2}(V_{11}^T L_{\varepsilon,1} + V_{12}^T L_{\varepsilon,2} + D_1^T V_{1\varepsilon,1} + D_2^T V_{1\varepsilon,2}). \end{aligned} \quad (47)$$

Here the monoclinic symmetry has already been used to obtain the asymptotically correct enthalpy in equation (44). The applied mechanical loads, temperature and electric fields should not vary rapidly over the plate surface, so that F , F_T and F_ε will be of desired orders to meet the requirement of asymptotical correctness.

4. Transforming into a Reissner–Mindlin model

Although equation (44) is asymptotically correct through the second order and use of this electric enthalpy expression is possible, it involves more complicated boundary conditions than necessary since it contains derivatives of the generalized strain measures. To obtain an enthalpy functional that is of practical use, one can transform the present approximation into a Reissner–Mindlin type model. It should be noted that fitting the asymptotic enthalpy into such a model is just one possible choice, and the possibility of fitting the same enthalpy into other more sophisticated 2D plate models exists.

In a Reissner–Mindlin model, there are two additional degrees of freedom, which are the transverse shear strains. These are incorporated into the rotation of transverse normal. If we introduce another triad \mathbf{B}_i^* for the deformed Reissner–Mindlin plate, the definition of 2D strains becomes

$$\begin{aligned} \mathbf{R}_{,\alpha} &= \mathbf{B}_\alpha^* + \varepsilon_{\alpha\beta}^* \mathbf{B}_\beta^* + 2\gamma_{\alpha 3}^* \mathbf{B}_3^* \\ \mathbf{B}_{i,\alpha}^* &= (-K_{\alpha\beta}^* \mathbf{B}_\beta^* \times \mathbf{B}_3^* + K_{\alpha 3}^* \mathbf{B}_3^*) \times \mathbf{B}_i^* \end{aligned} \quad (48)$$

where $\gamma = [2\gamma_{13} \quad 2\gamma_{23}]^T$, representing the transverse shear strains. One can express the classical strain measures ε in terms of the strain measures of the Reissner–Mindlin plate model as

$$\varepsilon = \mathcal{R} - \mathcal{D}_\alpha \gamma_{,\alpha} \quad (49)$$

where

$$\begin{aligned} D_1 &= \begin{bmatrix} 0 & 0 & 0 & 1 & 0 & 0 \\ 0 & 0 & 0 & 0 & 1 & 0 \end{bmatrix}^T \\ D_2 &= \begin{bmatrix} 0 & 0 & 0 & 0 & 1 & 0 \\ 0 & 0 & 0 & 0 & 0 & 1 \end{bmatrix}^T \end{aligned} \quad (50)$$

$$\mathcal{R} = [\varepsilon_{11}^* \quad 2\varepsilon_{12}^* \quad \varepsilon_{22}^* \quad K_{11}^* \quad K_{12}^* + K_{21}^* \quad K_{22}^*]^T.$$

Now one can express the electric enthalpy, equation (44), asymptotically correct to the second order, in terms of strains of the Reissner–Mindlin model as

$$\begin{aligned} 2\Pi_1 &= \mathcal{R}^T A \mathcal{R} - 2\mathcal{R}^T A D_\alpha \gamma_{,\alpha} + \mathcal{R}_{,1}^T B \mathcal{R}_{,1} + 2\mathcal{R}_{,1}^T C \mathcal{R}_{,2} \\ &+ \mathcal{R}_{,2}^T D \mathcal{R}_{,2} - 2\mathcal{R}^T F - 2\mathcal{R}^T F_T + 2\gamma_{,\alpha}^T D_\alpha N_T - 2\mathcal{R}^T F_\varepsilon \\ &+ 2\gamma_{,\alpha}^T D_\alpha N_\varepsilon. \end{aligned} \quad (51)$$

The generalized Reissner–Mindlin model used in the 2D thermopiezoelectric analysis is of the form

$$\begin{aligned} 2\Pi_{\mathcal{R}} &= \mathcal{R}^T A \mathcal{R} - 2\mathcal{R}^T (F_{\mathcal{R}} + F_{T\mathcal{R}} + F_{\varepsilon\mathcal{R}}) + \gamma^T G \gamma \\ &- 2\gamma^T (F_\gamma + F_{T\gamma} + F_{\varepsilon\gamma}). \end{aligned} \quad (52)$$

To find an equivalent Reissner–Mindlin model equation (52) for equation (51), one has to eliminate all partial derivatives of the classical 2D strain measures. The equilibrium equations are used to achieve this. From the two equilibrium equations balancing bending moments with applied moments m_α , which are calculated from equation (25), we find that

$$\begin{aligned} \mathcal{D}_\alpha^T (A \mathcal{R}_{,\alpha} - F_{\mathcal{R},\alpha} - F_{T\mathcal{R},\alpha} - F_{\varepsilon\mathcal{R},\alpha}) &= G \gamma - F_\gamma - F_{T\gamma} \\ &- F_{\varepsilon\gamma} - \begin{Bmatrix} m_1 \\ m_2 \end{Bmatrix}. \end{aligned} \quad (53)$$

Using equation (53), one can rewrite equation (51) as

$$\begin{aligned} 2\Pi_1 &= \mathcal{R}^T A \mathcal{R} + \gamma^T G \gamma - 2\mathcal{R}^T (F + F_T + F_\varepsilon) \\ &- 2\gamma^T \mathcal{D}_\alpha N_{T,\alpha} - 2\gamma^T \mathcal{D}_\alpha N_{\varepsilon,\alpha} + U^* \end{aligned} \quad (54)$$

where

$$U^* = \mathcal{R}_{,1}^T \bar{B} \mathcal{R}_{,1} + 2\mathcal{R}_{,1}^T \bar{C} \mathcal{R}_{,2} + \mathcal{R}_{,2}^T \bar{D} \mathcal{R}_{,2} \quad (55)$$

and

$$\begin{aligned} \bar{B} &= B + A D_1 G^{-1} D_1^T A \\ \bar{C} &= C + A D_1 G^{-1} D_2^T A \\ \bar{D} &= D + A D_2 G^{-1} D_2^T A. \end{aligned} \quad (56)$$

If we can drive U^* to zero for any \mathcal{R} , then we have found an asymptotically correct Reissner–Mindlin plate model. For generally anisotropic plates, however, this term cannot be driven to zero, but we can minimize the error to obtain a Reissner–Mindlin model that is as close to asymptotical correctness as possible. The accuracy of the Reissner–Mindlin model depends on how close to zero one can drive this term of the energy.

One could proceed with the optimization at this point, but there are only three unknowns, the elements of the shear stiffness matrix G . It is desirable to introduce more unknowns, if possible, into the optimization problem, and this can be safely done because, for a given order, we know that there is no unique plate theory [21]. Thus, one can relax the constraints in equation (5) to be $\langle w_i \rangle = \text{constant}$ and still obtain an asymptotically correct energy functional. Since the zeroth-order approximation gives us an asymptotic model corresponding to classical plate theory, we only relax the constraints for the first-order approximation. This relaxation will modify the warping field to be

$$\bar{V}_1 = V_{11}\varepsilon_{,1} + V_{12}\varepsilon_{,2} + V_{1L} + V_{1T} + V_{1\varepsilon} + L_1\varepsilon_{,1} + L_2\varepsilon_{,2} \quad (57)$$

where L_1, L_2 consist of 24 constants. The remaining energy U^* will also be modified to be

$$U^* = \mathcal{R}_{,1}^T \hat{B} \mathcal{R}_{,1} + 2\mathcal{R}_{,1}^T \hat{C} \mathcal{R}_{,2} + \mathcal{R}_{,2}^T \hat{D} \mathcal{R}_{,2} \quad (58)$$

and

$$\begin{aligned} \hat{B} &= \bar{B} + 2L_1^T D_1 \\ \hat{C} &= \bar{C} + (L_1^T D_2 + D_1^T L_2) \\ \hat{D} &= \bar{D} + 2L_2^T D_2. \end{aligned} \quad (59)$$

Since now we have 27 unknowns, the optimization is much more flexible. It can give us a more optimal solution for the shear stiffness matrix G to fit the second-order, asymptotically correct enthalpy into a Reissner–Mindlin model. In other words, when one carries out the optimization as described here, one finds the Reissner–Mindlin model that describes as closely as possible the 2D electric enthalpy that is asymptotically correct through the second order of h/l .

After minimizing U^* , the ‘best’ electric enthalpy to be used for the 2D plate Reissner–Mindlin model for the purposes of thermopiezoelectric analysis can be expressed as:

$$\begin{aligned} 2\Pi_{\mathcal{R}} &= \mathcal{R}^T A \mathcal{R} - 2\mathcal{R}^T (F + F_T + F_{\mathcal{E}}) + \gamma^T G \gamma \\ &\quad - 2\gamma^T \mathcal{D}_{\alpha} (N_{T,\alpha} + N_{\mathcal{E},\alpha}). \end{aligned} \quad (60)$$

5. Recovery relations

From the above, we have obtained a Reissner–Mindlin plate model that is as close as possible to being asymptotically correct in the sense of matching the electric enthalpy. The stiffness matrices A , G , load-related terms, and non-mechanical stress resultants can be used as input for a plate theory derived from the 2D electric enthalpy obtained here. The nonlinear theory presented in [20] is an appropriate choice, but some modification of the loading terms is required.

However, while it is necessary to accurately calculate the 2D displacement field of the plates, this is not sufficient in many applications. Ultimately, *the fidelity of a reduced-order model such as this depends on how well it can predict the 3D results in the original 3D problem*. Hence, recovery relations should be provided to complete the reduced-order model. By recovery relations, we mean expressions for 3D displacement, strain and stress fields in terms of 2D quantities and x_3 . For the purpose of validation, results obtained for the 3D field variables from the reduced-order model must be compared with those of the original 3D model.

For an energy that is asymptotically correct through the second order, we can recover the 3D displacement, strain and stress fields only through the first order in a strict sense of asymptotical correctness. Using equations (1), (3) and (4), one can recover the 3D displacement field through the first order as

$$U_{3d} = u_{2d} + x_3 \begin{Bmatrix} C_{31} \\ C_{32} \\ C_{33} - 1 \end{Bmatrix} + S V_0 + S \bar{V}_1 \quad (61)$$

where U_{3d} is the column matrix of 3D displacements, u_{2d} the plate displacements, and C_{ij} the components of global rotation tensor from equation (3). From equation (11), one can recover the 3D strain field through the first order as

$$\Gamma = \Gamma_h S (V_0 + \bar{V}_1) + \Gamma_{\epsilon} \epsilon + \Gamma_{l_1} S V_{0,1} + \Gamma_{l_2} S V_{0,2}. \quad (62)$$

Then, one can use the 3D constitutive relation

$$\sigma = D \Gamma - D \alpha T - D d \mathcal{E} \quad (63)$$

to obtain all six of the 3D stress components σ_{ij} .

Since we have obtained an optimum shear stiffness matrix G , some of the recovered 3D results through the first order are better than classical theory and conventional FOSDT. (Note that conventional FOSDT has no rational way to find the so-called shear correction factors.) However, the agreement is not satisfactory for the transverse normal stress σ_{33} . Let us recall that the Reissner–Mindlin theory that has been constructed only ensures a good fit with the asymptotically correct 3D displacement field of the first order (while energy is approximated to the second order). Thus, in order to obtain recovery relations that are valid to the same order as the energy, the VAM iteration needs to be applied one more time.

Using the same procedure listed in the previous section, the second-order warping can be obtained and expressed symbolically as

$$V_2 = V_{21\epsilon,11} + V_{22\epsilon,12} + V_{23\epsilon,22} + V_{2L} + V_{2T} + V_{2\mathcal{E}}. \quad (64)$$

Then we write the 3D recovery relations for displacement through the second order as

$$U_{3d} = u_{2d} + x_3 \begin{Bmatrix} C_{31} \\ C_{32} \\ C_{33} - 1 \end{Bmatrix} + S (V_0 + \bar{V}_1 + V_2) \quad (65)$$

and the strain field through the second order is

$$\begin{aligned} \Gamma &= \Gamma_h S (V_0 + \bar{V}_1 + V_2) + \Gamma_{\epsilon} \epsilon + \Gamma_{l_1} S (V_{0,1} + \bar{V}_{1,1}) \\ &\quad + \Gamma_{l_2} S (V_{0,2} + \bar{V}_{1,2}). \end{aligned} \quad (66)$$

Again the stresses through the second order can be obtained from the 3D constitutive law, equation (63).

6. Numerical examples

The computer program VAPAS has been extended to implement the present theory. Several numerical examples are given here to validate the proposed theory and code against the 3D thermopiezoelectricity solutions with one-way coupling that are specialized from [22].

First, to assess the asymptotical correctness of the proposed theory, we study a cylindrical bending problem for a single-layer plate made with a piezoelectric material with isotropic mechanical properties (E as the Young’s modulus, ν Poisson’s ratio) and d as the strain–piezoelectric constants in both directions of the reference plane. The plate is simply supported with width L along the x_1 axis (the ‘lateral’ direction) and infinitely long along the x_2 axis (the ‘longitudinal’ direction). The lower surface is grounded and the upper surface is applied with the following electric potential:

$$\phi = \phi_0 \sin\left(\frac{\pi x_1}{L}\right). \quad (67)$$

Let us assume the thickness of the plate is h , and the normalized thickness coordinate $\zeta = x_3/h$. Then, the small parameter used in our theory is

$$\delta = \frac{h}{l} = \frac{\pi h}{L}. \quad (68)$$

Table 1 lists the nontrivial displacements and stresses. The exact solutions are obtained based on [22] and expanded into

Table 1. Three-dimensional displacement and stresses under applied voltage.

Normalized lateral displacement $\left(\frac{U_1}{hd\phi_0}\right)$	
Exact	$-\frac{(\nu+1)}{\pi}\delta^{-1} - \frac{\pi(12\zeta^2-1)\nu}{24}\delta + \frac{\pi^3\nu[120\zeta^2(1-2\zeta^2)(\nu-2) + \nu+14]}{5760(\nu-1)}\delta^3 + o(\delta^4)$
Present	$-\frac{(\nu+1)}{\pi}\delta^{-1} - \frac{\pi(12\zeta^2-1)\nu}{24}\delta + o(\delta^2)$
Normalized transverse displacement $\left(\frac{U_3}{hd\phi_0}\right)$	
Exact	$\nu\zeta + \frac{\pi^2\zeta(4\zeta^2-1)\nu^2}{24(\nu-1)}\delta^2 + \frac{\pi^4\zeta\nu[8\zeta^2(6\zeta^2-5)(\nu+1) - \nu+15]}{5760(\nu-1)}\delta^4 + o(\delta^4)$
Present	$\nu\zeta + \frac{\pi^2\zeta(4\zeta^2-1)\nu^2}{24(\nu-1)}\delta^2 + o(\delta^2)$
Normalized lateral in-plane stress $\left(\frac{\sigma_{11}}{Ed\phi_0}\right)$	
Exact	$-\frac{\pi^2(12\zeta^2-1)\nu}{24(\nu^2-1)}\delta^2 - \frac{\pi^4(240\zeta^4-120\zeta^2+7)\nu}{2880(\nu^2-1)}\delta^4 + o(\delta^4)$
Present	$-\frac{\pi^2(12\zeta^2-1)\nu}{24(\nu^2-1)}\delta^2 + o(\delta^2)$
Normalized longitudinal in-plane stress $\left(\frac{\sigma_{22}}{Ed\phi_0}\right)$	
Exact	$-1 - \frac{\pi^2(12\zeta^2-1)\nu^2}{24(\nu^2-1)}\delta^2 + \frac{\pi^4(-240\zeta^4+120\zeta^2+1)\nu^2}{5760(\nu^2-1)}\delta^4 + o(\delta^4)$
Present	$-1 - \frac{\pi^2(12\zeta^2-1)\nu^2}{24(\nu^2-1)}\delta^2 + o(\delta^2)$
Normalized lateral transverse shear stress $\left(\frac{\sigma_{13}}{Ed\phi_0}\right)$	
Exact	$\frac{\pi^3\zeta(4\zeta^2-1)\nu}{24(\nu^2-1)}\delta^3 + o(\delta^4)$
Present	Not available
Normalized lateral transverse shear stress $\left(\frac{\sigma_{33}}{Ed\phi_0}\right)$	
Exact	$\frac{\pi^4(4\zeta^2-1)^2\nu}{384(\nu^2-1)}\delta^4 + o(\delta^4)$
Present	Not available

a series in terms of δ with $o(*)$ denoting terms asymptotically smaller than the order of $*$. The present theory can predict the correct results up to the second order of δ with respect to the leading terms for each of the 3D quantities, which clearly demonstrate that our theory is asymptotically correct up to the second order for this particular problem, although the prediction of transverse components for this problem, because of their high order, is outside the scope of our theory.

However, this should not mislead the reader to assume that the present theory is asymptotically correct up to the second order in general. Because of the loss of some information in the conversion to a Reissner–Mindlin model, the present theory is at best asymptotically correct through the second order for particular cases. For the general case, however, the theory can only be interpreted as that Reissner–Mindlin model which is the closest to being asymptotically correct. To illustrate the above statement, we provide results for the same piezoelectric plate under transverse surface mechanical loads given by

$$\tau_3 = \beta_3 = \frac{p_0}{2} \sin\left(\frac{\pi x_1}{L}\right) \quad (69)$$

in addition to the aforementioned electric potential in equation (67). Table 2 only lists the nontrivial displacement results. One can observe from table 2 that there is a slight difference for the second-order prediction (relative to the dominant terms) between the present theory and exact solution. It is interesting to note that if one sets ν equal to zero the difference disappears. Evidently some information belonging to the second order and indeed included in the asymptotically correct enthalpy cannot be captured in a Reissner–Mindlin model. When we transform the asymptotically correct model into a Reissner–Mindlin model, this information is lost.

However, since the loss is small in comparison to the dominant terms, the numerical difference between the present theory and the exact solution is expected to be small. To verify this expectation, we will present some numerical results for piezoelectric plates to demonstrate the accuracy of our theory.

Table 2. Three-dimensional displacements under both mechanical and electric loads. (Note: $\hat{U}_{\text{diff}} = \frac{4hp_0\xi v(33v^5 - 7v^4 + 58v^3 + 58v^2 - 11v + 29)}{5E\pi(11v^4 - 12v^3 + 34v^2 - 12v + 11)}$.)

Normalized lateral displacement (U_1)	
Exact	$\frac{12hp_0\xi(v^2 - 1)}{E\pi^3}\delta^{-3} + \frac{h(v + 1)\{p_0\xi[(20v - 40)\xi^2 + 9v + 6 - 10Ed\phi_0]\}}{10E\pi}\delta^{-1} + o(\delta^{-1})$
Present	$\frac{12hp_0\xi(v^2 - 1)}{E\pi^3}\delta^{-3} + \left(\frac{h(v + 1)\{p_0\xi[(20v - 40)\xi^2 + 9v + 6 - 10Ed\phi_0]\}}{10E\pi} + \hat{U}_{\text{diff}}\right)\delta^{-1} + o(\delta^{-1})$
Normalized transverse displacement (U_3)	
Exact	$\frac{12hp_0(v^2 - 1)}{E\pi^4}\delta^{-4} - \frac{3hp_0(v + 1)[(20\xi^2 + 3)v - 8]}{10E\pi^2}\delta^{-2} + o(\delta^{-2})$
Present	$\frac{12hp_0(v^2 - 1)}{E\pi^4}\delta^{-4} - \left(\frac{3hp_0(v + 1)[(20\xi^2 + 3)v - 8]}{10E\pi^2} + \hat{U}_{\text{diff}}\right)\delta^{-2} + o(\delta^{-2})$

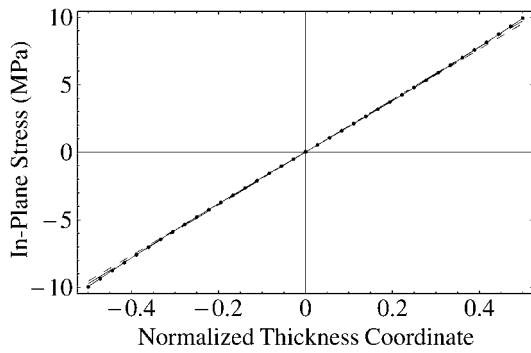


Figure 2. Distribution of the 3D stress σ_{11} versus the thickness coordinate. Solid line: exact solution; dots: VAPAS; dashed line: FOSDT; long-dash/short-dash line: CLT.

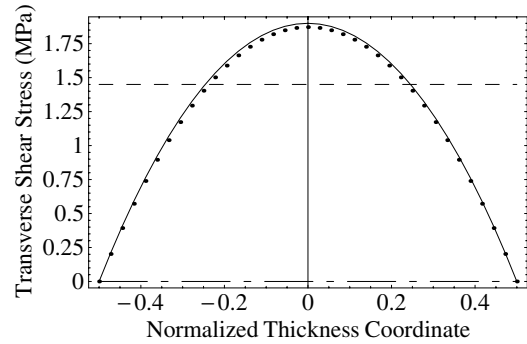


Figure 4. Distribution of the 3D stress σ_{13} versus the thickness coordinate. Solid line: exact solution; dots: VAPAS; dashed line: FOSDT; long-dash/short-dash line: CLT.

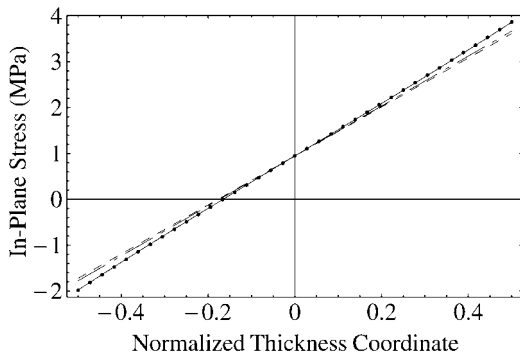


Figure 3. Distribution of the 3D stress σ_{22} versus the thickness coordinate. Solid line: exact solution; dots: VAPAS; dashed line: FOSDT; long-dash/short-dash line: CLT.

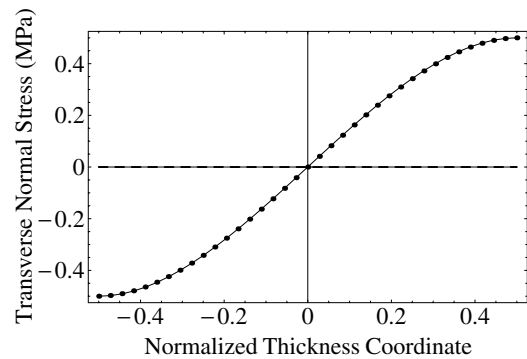


Figure 5. Distribution of the 3D stress σ_{33} versus the thickness coordinate. Solid line: exact solution; dots: VAPAS; dashed line: FOSDT; long-dash/short-dash line: CLT.

We study a single-layer plate with $h = 1$ mm and $L = 4$ mm under the applied voltage as in equation (67) with $\phi_0 = 100$ V and mechanical load on the surfaces as in equation (69) with $p_0 = 1$ MPa. The piezoelectric material properties are taken from [8]

$$\begin{aligned}
 E_L &= E_T = 63 \text{ GPa} \\
 G_{LT} &= G_{TT} = 24.6 \text{ GPa} \\
 \nu_{LT} &= \nu_{TT} = 0.28 \\
 d_{113} &= d_{223} = 150 \times 10^{-12} \text{ m V}^{-1}.
 \end{aligned}
 \tag{70}$$

Figures 2–5 plot the nontrivial components of 3D stress distribution through the thickness. (Note that, because the 2D variables are either sine or cosine functions of x_1 , $\sigma_{\alpha\beta}$ and σ_{33} are plotted for the position $x_1 = L/2$, and $\sigma_{\alpha 3}$ are plotted for the position $x_1 = 0$ or L .) One can observe that VAPAS results are almost on the top of exact solutions and are much better than the results of CLT and FOSDT. The loss of information is evidently negligible in this case.

The computational cost of the present theory is the same as a first-order, single-layer theory. However, it can achieve an accuracy comparable to higher-order layerwise theories. To demonstrate this, we study a more challenging and realistic

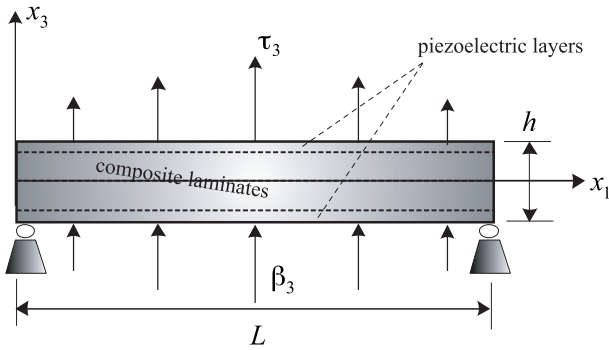


Figure 6. Sketch of a four-layer smart plate.

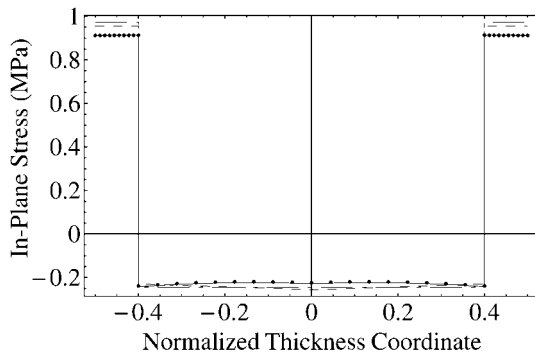


Figure 7. Distribution of the 3D stress σ_{11} versus the thickness coordinate. Solid line: exact solution; dots: VAPAS; dashed line: FOSDT; long-dash/short-dash line: CLT.

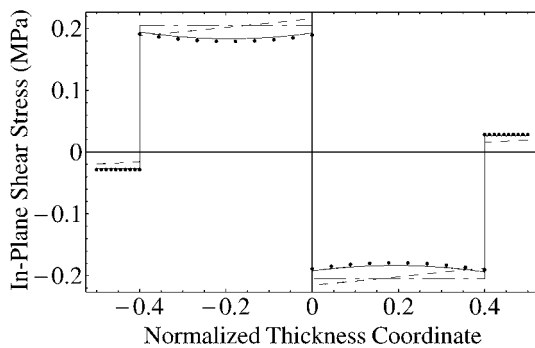


Figure 8. Distribution of the 3D stress σ_{12} versus the thickness coordinate. Solid line: exact solution; dots: VAPAS; dashed line: FOSDT; long-dash/short-dash line: CLT.

problem. It is a four-layer piezoelectric plate with $h = 1$ mm and $L = 10$ mm (see figure 6). The two face sheets are made from a piezoelectric material with properties as in equation (70) and the inside layers are normal graphite/epoxy composites with the following properties:

$$\begin{aligned} E_L &= 172 \text{ GPa} & E_T &= 6.9 \text{ GPa} \\ G_{LT} &= 3.4 \text{ GPa} & G_{TT} &= 1.4 \text{ GPa} \\ \nu_{LT} &= 0.25 & \nu_{TT} &= 0.25. \end{aligned} \quad (71)$$

The piezoelectric layers are each 0.1 mm thick, and the regular composite layers are each 0.4 mm thick. The layup scheme is $[0^\circ/-45^\circ/45^\circ/0^\circ]$ from bottom to top. An electric potential

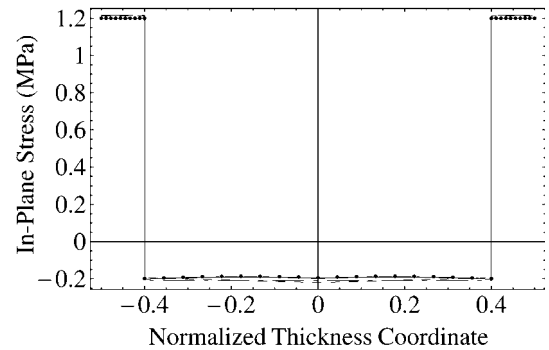


Figure 9. Distribution of the 3D stress σ_{22} versus the thickness coordinate. Solid line: exact solution; dots: VAPAS; dashed line: FOSDT; long-dash/short-dash line: CLT.

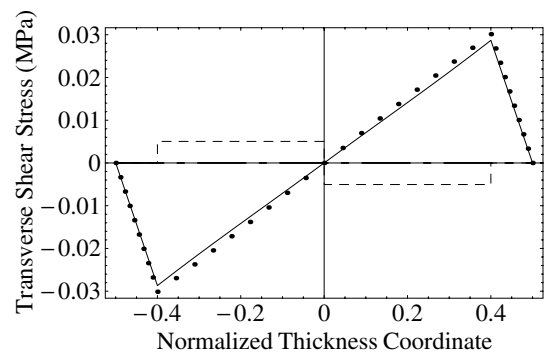


Figure 10. Distribution of the 3D stress σ_{13} versus the thickness coordinate. Solid line: exact solution; dots: VAPAS; dashed line: FOSDT; long-dash/short-dash line: CLT.

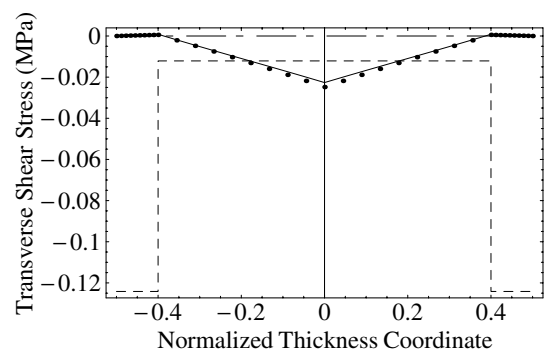


Figure 11. Distribution of the 3D stress σ_{23} versus the thickness coordinate. Solid line: exact solution; dots: VAPAS; dashed line: FOSDT; long-dash/short-dash line: CLT.

according to equation (67) with $\phi_0 = 10$ V is applied to the upper surfaces of both piezoelectric layers. The recovered stresses are plotted in figures 7–12. Again, there is excellent agreement between results from VAPAS and the exact solution. This excellent agreement even includes the transverse normal stress, although this stress component is very small relative to other components.

To investigate the behavior of a piezoelectric plate under a combination of different kinds of loads, we apply a mechanical load according to equation (69) with $p_0 = 1$ MPa onto the surfaces. All the components of the stress due to the combination of these two loads are plotted in figures 13–18.

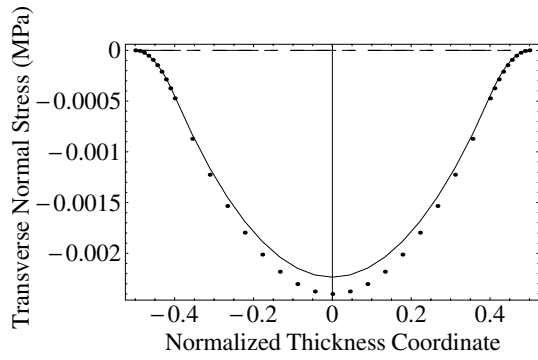


Figure 12. Distribution of the 3D stress σ_{33} versus the thickness coordinate. Solid line: exact solution; dots: VAPAS; dashed line: FOSDT; long-dash/short-dash line: CLT.

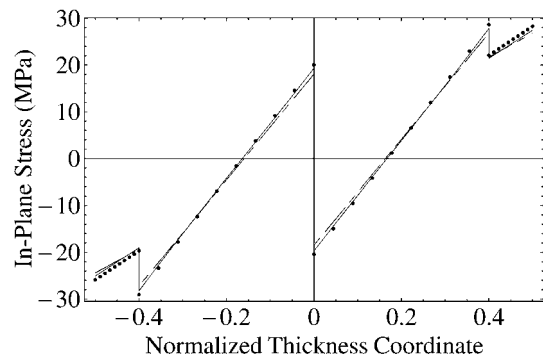


Figure 15. Distribution of the 3D stress σ_{22} versus the thickness coordinate. Solid line: exact solution; dots: VAPAS; dashed line: FOSDT; long-dash/short-dash line: CLT.

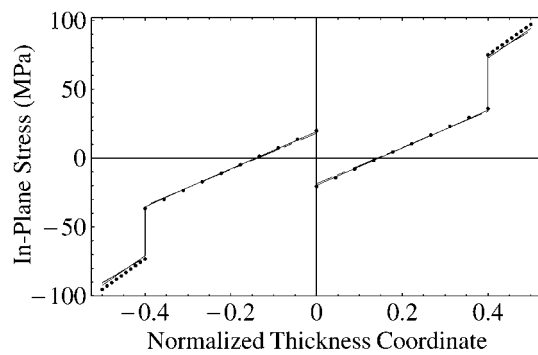


Figure 13. Distribution of the 3D stress σ_{11} versus the thickness coordinate. Solid line: exact solution; dots: VAPAS; dashed line: FOSDT; long-dash/short-dash line: CLT.

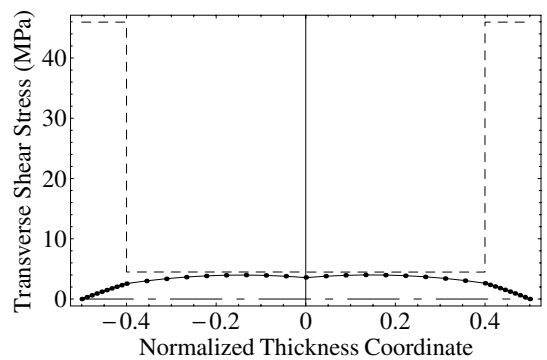


Figure 16. Distribution of the 3D stress σ_{13} versus the thickness coordinate. Solid line: exact solution; dots: VAPAS; dashed line: FOSDT; long-dash/short-dash line: CLT.

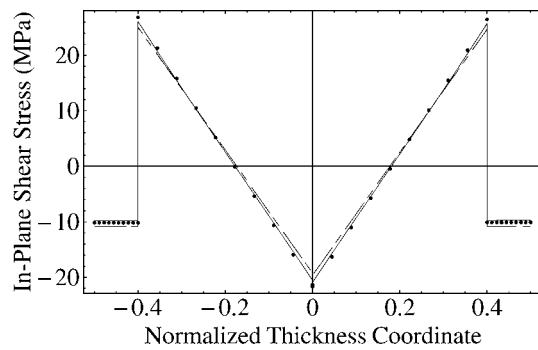


Figure 14. Distribution of the 3D stress σ_{12} versus the thickness coordinate. Solid line: exact solution; dots: VAPAS; dashed line: FOSDT; long-dash/short-dash line: CLT.

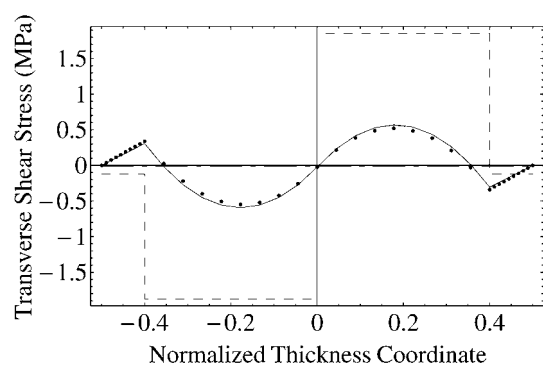


Figure 17. Distribution of the 3D stress σ_{23} versus the thickness coordinate. Solid line: exact solution; dots: VAPAS; dashed line: FOSDT; long-dash/short-dash line: CLT.

VAPAS achieves excellent agreement with the exact solution for all six stress components, including the transverse normal stress. Such excellent agreement is not found in the literature, and even those higher-order layer theories that have many more degrees of freedom, the number of which is dependent on the number of layers, do not provide predictions of the 3D stresses as accurate as those obtained from VAPAS. The thermoelastic behavior of composite plates has been studied in [16]. The current version of VAPAS can reproduce all the results there. No additional examples will be given here for the sake of brevity.

It is noted that the above examples are greatly simplified. They are presented for the only purpose of validation, which is a conventional way of validating approximate models for composite structures. However, the present theory is formulated with sufficient generality to carry out a thermopiezoelectric analysis for arbitrary composite laminated piezoelectric plates, the layers of which are made with monoclinic materials. One may use VAPAS along with a 2D plate solver to analyze more realistic composite piezoelectric plates.

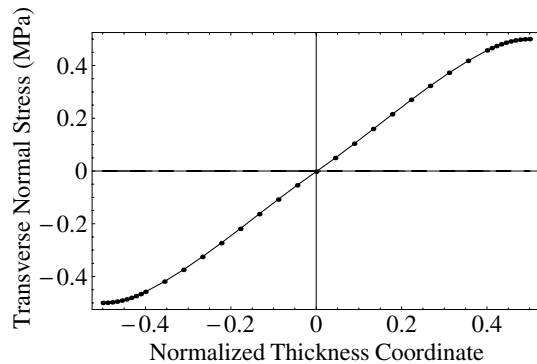


Figure 18. Distribution of the 3D stress σ_{33} versus the thickness coordinate. Solid line: exact solution; dots: VAPAS; dashed line: FOSDT; long-dash/short-dash line: CLT.

7. Conclusion

A thermopiezoelectric model of composite piezoelectric plates has been developed by use of the variational-asymptotic method. A 2D constitutive law in the form of a Reissner–Mindlin plate model, that is as close to asymptotical correctness as possible, has been obtained by solving the 1D through-the-thickness analysis. The original 3D results have been accurately reproduced from a Reissner–Mindlin type plate analysis. Numerical examples show that, although the resulting theory is as simple and efficient as a single-layer, first-order shear–deformation theory, it can approximate the 3D exact solution with extremely high accuracy.

The present work differs from previous work on this topic in the literature in the following four aspects:

- (i) The present formulation is in an intrinsic form which is suitable for both geometrically linear and nonlinear plate theories.
- (ii) Without using any ad hoc kinematical assumptions, the dimensional reduction from 3D to 2D is carried out systematically by using the variational-asymptotic method.
- (iii) The Reissner–Mindlin type model proposed in the present theory is *not* a first-order shear–deformation theory. The present theory differs from such theories in that all possible deformations are represented in terms of the 3D warping functions, including those which are purposely eliminated in the development of first-order shear–deformation theories. These warping functions are obtained by use of the variational-asymptotic method.
- (iv) The present theory decouples the modeling process of the plate completely from the 2D plate problem described on the reference plane so that the obtained 2D generalized constitutive model can be used as input for any other 2D standard plate solver. The ease with which VAPAS may be connected to a standard plate or shell solver, and the confidence one can have in the accuracy of the recovered stress and strain, allow the structural analyst focus on solving the 2D problem for different situations.

The computer program VAPAS can now be used along with a 2D Reissner–Mindlin type plate solver to perform an efficient yet accurate analysis for thermopiezoelectric behavior

of composite piezoelectric plates. Such a tool will be very useful for designers of smart plates to carry out accurate tradeoff studies more efficiently. It has to be emphasized that the present work only deals with thermal and/or piezoelectric actuation of smart plates. Changes of temperature and electric fields caused by deformation of the plate, which is the so-called sensing capability of smart plates, cannot be treated by means of the present theory. To extend the theory to deal with this class of problems is possible but requires significant effort.

Acknowledgments

This research was supported in part by the Air Force Office of Scientific Research, USAF, under grant F49620-01-1-0038 (Major William M Hilbun, technical monitor). The views and conclusions contained herein are those of the authors and should not be interpreted as necessarily representing the official policies or endorsement, either expressed or implied, of AFOSR or the US Government.

References

- [1] Loewy R G 1997 Recent developments in smart structures with aeronautical applications *Smart Mater. Struct.* **6** R11–42
- [2] Saravanan D A and Heyliger P R 1999 Mechanics and computational models for laminated piezoelectric beams, plates, and shells *Appl. Mech. Rev.* **52** 305–19
- [3] Tauchert T R, Ashida F, Noda N, Adali S and Verijenko V 2000 Developments in thermopiezoelectricity with relevance to smart composite structures *Compos. Struct.* **48** 31–8
- [4] Chopra I 2000 Status of application of smart structures technology to rotorcraft systems *J. Am. Helicopter Soc.* **45** 228–52
- [5] Giurgiutiu V 2000 Review of smart materials actuation solutions for aeroelastic and vibration control *J. Intell. Mater. Syst. Struct.* **11** 525–44
- [6] Tauchert T R 1992 Piezothermoelastic behavior of a laminated plate *J. Therm. Stresses* **15** 25–37
- [7] Lee H-J and Saravanan D A 1997 Generalized finite element formulation for smart multilayered thermal piezoelectric composite plates *Int. J. Solids Struct.* **34** 3355–71
- [8] Chattopadhyay A, Li J and Gu H 1999 Coupled thermo–piezoelectric–mechanical model for smart composite laminates *AIAA J.* **37** 1633–8
- [9] Lee C K 1990 Theory of laminated piezoelectric plates for the design of distributed sensors/actuators *J. Acoust. Soc. Am.* **87** 1144–58
- [10] Tzou H S and Zhong J P 1993 Electromechanics and vibrations of piezoelectric shell distributed systems *J. Dyn. Syst. Meas. Control* **115** 506–17
- [11] Oh J and Cho M 2004 A finite element based on cubic zig-zag plate theory for the prediction of thermo–electric–mechanical behaviors *Int. J. Solids Struct.* **41** 1357–75
- [12] Mitchell J A and Reddy J N 1995 A refined hybrid plate theory for composite laminates with piezoelectric laminae *Int. J. Solids Struct.* **32** 2345–67
- [13] Yu W, Hodges D H and Volovoi V V 2002 Asymptotic construction of Reissner-like models for composite plates with accurate strain recovery *Int. J. Solids Struct.* **39** 5185–203
- [14] Yu W, Hodges D H and Volovoi V V 2003 Asymptotically accurate 3D recovery from Reissner-like composite plate finite elements *Comput. Struct.* **81** 439–54
- [15] Yu W, Hodges D H and Volovoi V V 2002 Asymptotic generalization of Reissner–Mindlin theory: accurate

- three-dimensional recovery for composite shells *Comput. Methods Appl. Mech. Eng.* **191** 5087–109
- [16] Yu W and Hodges D H 2004 An asymptotic approach for thermoelastic analysis of laminated composite plates *J. Eng. Mech.* **130** 531–40 (<http://www.mae.usu.edu/faculty/wenbin/papers/thermoplate.pdf>)
- [17] Berdichevsky V L 1979 Variational-asymptotic method of constructing a theory of shells *Prikl. Matem. Mekh.* **43** 664–87
- [18] Danielson D A 1991 Finite rotation with small strain in beams and plates *Proc. 2nd Pan Am. Congr. of Appl. Mech. (Valparaiso, Chile, January 1991)*
- [19] Danielson D A and Hodges D H 1987 Nonlinear beam kinematics by decomposition of the rotation tensor *J. Appl. Mech.* **54** 258–62
- [20] Hodges D H, Atilgan A R and Danielson D A 1993 A geometrically nonlinear theory of elastic plates *J. Appl. Mech.* **60** 109–16
- [21] Sutyurin V G and Hodges D H 1996 On asymptotically correct linear laminated plate theory *Int. J. Solids Struct.* **33** 3649–71
- [22] Shang F, Wang Z and Li Z 1997 Analysis of thermally induced cylindrical flexure of laminated plates with piezoelectric layers *Composites B* **28** 185–93